Relevance of Thermal Effects in the Formation of Endohedral Metallofullerenes: The Case of Gd$_3$N@C_s(39663)-C$_{82}$ and Other Related Systems[†]

Marc Mulet-Gas,[‡] Antonio Rodríguez-Fortea,*,[‡] Luis Echegoyen,[§] and Josep M. Poblet*,[‡]

[‡]Departament de Química Física i Inorgànica, Universitat Rovira i Virgili, C/Marcel·lí Domingo, s/n 43007 Tarragona, Spain
[§]Department of Chemistry, University of Texas at El Paso, El Paso, Texas 79968, United States

S *Supporting Information*

ABSTRACT: Thermal contributions to the free energy have to be taken into account to rationalize the formation of Gd$_3$N@C_s(39663)-C$_{82}$, a nitride endohedral metallofullerene that shows a carbon cage with two fused pentagons which is not predicted to have the lowest electronic energy among the isomers of C$_{82}$. The lower symmetry and the larger number of pyracylene units of C_s(39663)-C$_{82}$ with respect to the cage in the lowest-energy metallofullerene, C_{2v}(39705)-C$_{82}$, favor its formation at high temperatures, as seen for other similar cage isomers that encapsulate metal clusters within the C$_{80}$ and C$_{82}$ families. These cages, which share common motifs with the prototypical I_h(7)-C$_{80}$, are all related by C$_2$ insertions/extrusions and Stone−Wales transformations.
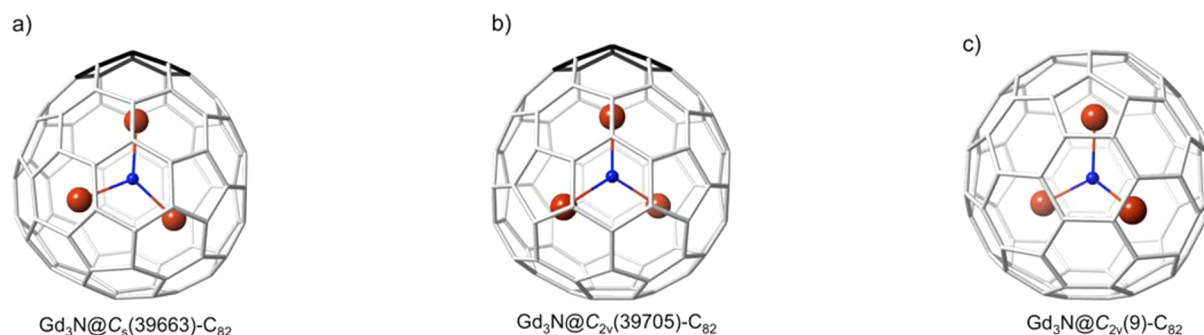

Gd$_3$N@C_s(39663)-C$_{82}$
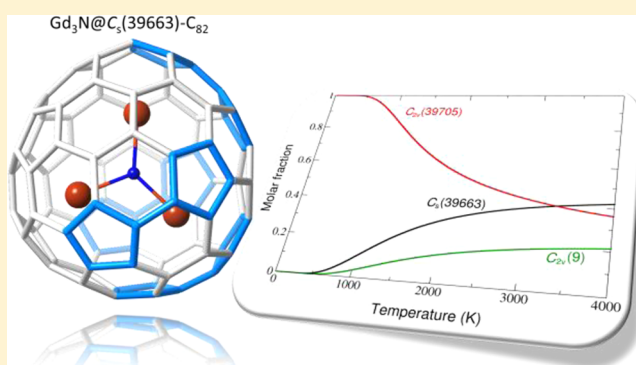
■ INTRODUCTION

Endohedral metallofullerenes (EMFs), that is, carbon cages with one or more metal atoms or metal clusters trapped inside, have been intensively studied during the past decade because of their interesting properties that could be of use in different fields such as medicine and materials sciences.[1−3] The discovery of Sc$_3$N@C$_{80}$, the third most abundant fullerene after C$_{60}$ and C$_{70}$, by Dorn and co-workers in 1999 represented the beginning of a new field in the chemistry of fullerenes.[4] Since then, a large number of nitride EMFs with Group 3 metals or Lanthanides as well as carbide, oxide, sulfide, and classical (M or M$_2$) EMFs have been isolated and characterized.[1,5−7] The electronic structure of these EMFs can be easily rationalized using an ionic model of interaction. For instance, in nitride EMFs there is a formal transfer of six electrons from the metal cluster to the carbon cage, (M$_3$N)$^{6+}$@(C$_{2n}$)$^{6−}$.[6,8] Such a charge transfer changes the relative stabilities of the C$_{2n}$ isomers, and the cages that encapsulate are usually structural isomers of the most-stable hollow cages; even in some cases they do not fulfill the so-called *isolated pentagon rule* (IPR).[9] Predictions of the isomer cages that are suitable to encapsulate the metal nitride either by checking the molecular orbital energies of the hollow cages[10,11] or by computing the stability of anionic cages are well established.[8] A topological rule that provides a physical explanation for the selection of a particular host cage by a given cluster has been recently formulated.[12] The *maximum pentagon separation rule* states that the most suitable candidates to entrap metal clusters are those cages with the largest separation among pentagons, which localize more negative charge than hexagons, so as to minimize Coulomb repulsions.

The simple rules derived from the ionic model are able to explain the relative stabilities and abundances of a large number of EMFs. However, the electronic energies at 0 K cannot justify the experimental results for other EMFs. Slanina demonstrated that the Gibbs energy has to be taken into account to incorporate the effect of the high temperatures that are used to synthesize the fullerenes.[13] For instance, the amount of the minor isomer Sc$_3$N@D_{5h}-C$_{80}$ (between 10 and 20% of the total Sc$_3$N@C$_{80}$) relative to Sc$_3$N@I_h-C$_{80}$ in the electric-arc synthesis can only be explained by taking into account the thermal effects.[14] We have shown recently that the oxide EMF Sc$_2$(μ-O)@C_s(6)-C$_{82}$ is the first example in which the relevance of the thermal and entropic contributions to the stability of the fullerene isomer has been confirmed through the characterization of the X-ray structure.[15] Sc$_2$(μ_2-O)@C_{3v}(8)-C$_{82}$ is predicted to be the most abundant product at low temperatures, but Sc$_2$(μ_2-O)@C_s(6)-C$_{82}$ is more favored when thermal effects are taken into account and becomes the most abundant species at higher temperatures (above 1200 K). Analogous studies with the C_s(6), C_{3v}(8), and C_{2v}(9) isomers of Sc$_2$(μ_2-S)@C$_{82}$ confirmed the fact that both C_s(6) and C_{3v}(8) cages are observed.[16] Similar results are also predicted for empty fullerenes. For instance, Slanina found that while the lowest-energy IPR isomer for C$_{80}$ is D_{5d}(1), at synthetic conditions the

Figure 1. Structures of the three isomers of Gd$_3$N@C$_{82}$, with the non-IPR C_s(39663)-C$_{82}$ (a), the non-IPR C_{2v}(39705)-C$_{82}$ (b), and the IPR C_{2v}(9)-C$_{82}$ (c) cages. The pentalene unit in the two non-IPR structures is highlighted in black.

D_2(2) isomer is the most abundant one,[17] as confirmed later by NMR experiments.[18,19]

Recently, X-ray diffraction experiments have unambiguously shown that the carbon cage in Gd$_3$N@C$_{82}$ is the egg-shaped non-IPR C_s(39663)-C$_{82}$ isomer (Figure 1),[20] which is neither the lowest-energy hexaanion nor gives the most stable nitride EMF for M = Sc and Y, as shown by the computations of Popov and Dunsch.[8] We herein study the different isomers of Gd$_3$N@C$_{82}$ to assess the relevance of thermal contributions to their relative stabilities to understand why Gd$_3$N@C_s(39663)-C$_{82}$ is the cage experimentally observed. We also analyze the relationship between C_s(39663)-C$_{82}$ and other IPR and non-IPR cages that encapsulate metal clusters of the C$_{80}$, C$_{82}$, and C$_{84}$ families.

COMPUTATIONAL DETAILS

The calculations were conducted using density functional theory (DFT) methodology with the ADF 2009 program.[21,22] The exchange-correlation functionals of Becke[23] and Perdew[24] (BP86) were used for geometry optimizations and frequency calculations. Relativistic corrections were included by means of the ZORA formalism. Slater TZP basis sets were employed to describe the valence electrons. Frozen cores consisting of the 1s shell for C and N and the 1s to 4d shells for Gd were described by means of single Slater functions. All the Gd$_3$N@C$_{82}$ systems have been computed in their high spin electronic state (21 unpaired electrons). The revPBE[25] and B3LYP[26] functionals as well as the D3 dispersion corrections by Grimme[27] were also used to compute the relative energies of Gd$_3$N@C_s(39663)-C$_{82}$ with respect to C_{2v}(39705)-C$_{82}$ at 0 K. Frequency calculations for Y$_3$N@C$_{82}$ models, using the B3LYP functional and a TZP basis for Y (with the Stoll−Preuss pseudopotential)[28] and all-electron DZP basis sets for C and N, were also done (Turbomole code, version 6.3).[29] The numeration of the different isomers within a C$_{2n}$ family follows the spiral algorithm proposed by Fowler and Manolopoulos.[9]

RESULTS AND DISCUSSION

We have computed the free energies using the rigid rotor and harmonic oscillator approximation (RRHO) at different temperatures as well as their molar fractions derived from the free-energy calculations as done by Slanina and co-workers.[13] We have analyzed three isomers of Gd$_3$N@C$_{82}$, the non-IPR C_s(39663)-C$_{82}$ and C_{2v}(39705)-C$_{82}$, and the IPR C_{2v}(9)-C$_{82}$ cages, which are the three lowest-energy structures predicted by Popov and Dunsch for Y$_3$N@C$_{82}$,[8] a system that has been shown to be a good model for Gd$_3$N@C$_{82}$.[30] Isomer Gd$_3$N@C_{2v}(39705)-C$_{82}$ has the lowest energy at 0 K, with a difference of 6.2 and 8.0 kcal·mol^{-1} (BP86/TZP) compared to Gd$_3$N@C_s(39663)-C$_{82}$ and Gd$_3$N@C_{2v}(9)-C$_{82}$, respectively. The contribution of the zero-point energy vibrational correction to the relative stabilities is not very important (Table 1, second

Table 1. Relative Stabilities for the Three Isomers of Gd$_3$N@C$_{82}$[a,b]

	C_s(39663)	C_{2v}(39705)	C_{2v}(9)
ΔE (0 K)	6.2	0.0	8.0
ΔH (0 K)	6.1	0.0	7.3
ΔG (1000 K)	4.4	0.0	7.1
ΔG (2000 K)	2.6	0.0	6.4
ΔG (3000 K)	0.8	0.0	5.6
ΔG (4000 K)	−1.0	0.0	4.9

[a]Relative energies are in kcal·mol^{-1}. [b]The FEM model is considered to compute the free energies.

row). The C_{2v}(39705)-C$_{82}$ isomer is the most stable EMF even when the thermal and entropic effects are taken into account within the RRHO approximation. A modified treatment based on the idea that the encapsulated cluster can exercise large amplitude motions, especially at high temperatures, was also used.[13] Within this approximation, called the free, fluctuating or floating encapsulated model (FEM), which better reproduces the experimental results,[14−16] the stability of the Gd$_3$N@C_s(39663)-C$_{82}$ isomer increases at high temperatures, becoming the most abundant isomer at around 3400 K (see Table 1 and Figure 2). Although the predicted crossing temperature for the predominance of Gd$_3$N@C_s(39663)-C$_{82}$ is somewhat high, the important result is that the experimentally observed Gd$_3$N@C_s(39663)-C$_{82}$ is the favored isomer at high temperatures. The use of other density functionals, for instance those that include the exact exchange or additional dispersion
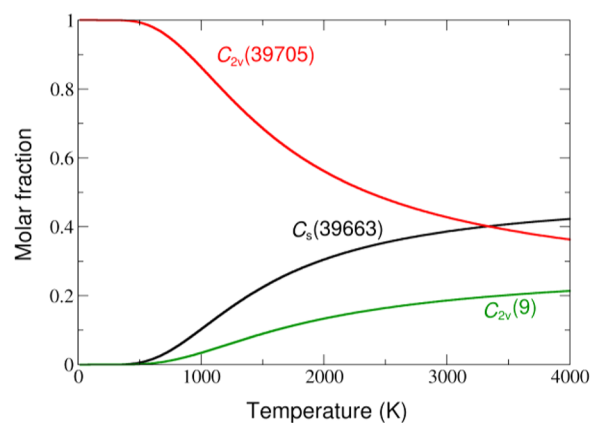
Figure 2. Plot of the computed molar fractions within the FEM model for Gd$_3$N@C_s(39663)-C$_{82}$, Gd$_3$N@C_{2v}(39705)-C$_{82}$ and Gd$_3$N@C_{2v}(9)-C$_{82}$ isomers.

corrections, to optimize the geometries and/or to compute the frequencies may provide lower crossing temperatures, in better agreement with experiments than the BP86/TZP results, but probably with the same qualitative information predicted here, that is, the inclusion of thermal effects are compulsory to understand the formation of $Gd_3N@C_s(39663)\text{-}C_{82}$, which is the favored isomer at high temperatures.

We have also estimated the relative energies at 0 K, ΔE (0K), between the two lowest-energy isomers using other density functionals (Table 2). The revPBE functional, also of the GGA

Table 2. Relative Energies of $Gd_3N@C_s(39663)\text{-}C_{82}$ with Respect to $C_{2v}(39705)\text{-}C_{82}$ at 0 K, ΔE (0 K), As Computed with Different Density Functionals[a]

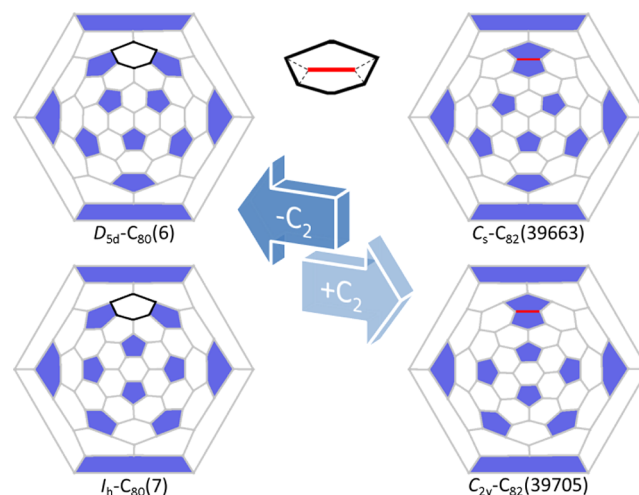|	$C_s(39663)$	$C_{2v}(39705)$
BP86	6.2	0.0
revPBE	6.2	0.0
B3LYP[b]	6.9	0.0
BP86-D3	6.0	0.0

[a]Relative energies are in kcal·mol^{-1}. [b]Single-point calculation on the BP86/TZP geometry.

type, leads to the same energy difference as BP86. The energy difference is somewhat larger (6.9 kcal·mol^{-1}) when the hybrid B3LYP functional is used. However, when including the dispersion corrections in the BP86 functional according to the D3 method by Grimme, the difference is slightly reduced to 6.0 kcal·mol^{-1}. Moreover, we have computed the frequencies at the B3LYP level for the model compounds $Y_3N@C_s(39663)\text{-}C_{82}$ and $Y_3N@C_{2v}(39705)\text{-}C_{82}$. We have made this approximation because of the difficulties (convergence problems, larger computational cost) to obtain the frequencies at this level for the Gd endohedral fullerenes. Although one could argue that Gd (157.25) is much heavier than Y (88.91) and hence vibrational frequencies of $Gd_3N@C_{82}$ involving metal atoms must be lower than those in $Y_3N@C_{82}$, we have checked that this approximation is totally valid. The main reason is that most of the normal modes of vibration that involve metal atoms, which show the lowest frequencies, are not taken into consideration within the FEM approximation (see Supporting Information for a more detailed explanation).

The predictions for the molar fractions of $Gd_3N@C_s(39663)\text{-}C_{82}$ and $Gd_3N@C_{2v}(39705)\text{-}C_{82}$ using the frequencies computed for the Y models at the above-mentioned computational level combined with the energy difference

obtained with BP86/TZP (6.2 kcal·mol^{-1}) and with BP86-D3/TZP (6.0 kcal·mol^{-1}) decreases the crossing temperature to 3090 and 2990 K, respectively.

At this point, it is worth remarking about the structural resemblance that the two lowest-energy non-IPR $C_s(39663)\text{-}C_{82}$ and $C_{2v}(39705)\text{-}C_{82}$ cages show. The two structures are related by a 36-degree rotation of a pentagonal motif, as can be seen in Figure 3. This small structural change, however, does not mean that the interconversion between the two structures is energetically feasible. High-energy barriers would have to be surmounted to break the C−C bonds to allow this rotation. Figure 4 shows that each of these non-IPR EMFs is also

Figure 4. Schematic two-dimensional representations of the relationship between the non-IPR $C_s(39663)\text{-}C_{82}$ and $C_{2v}(39705)\text{-}C_{82}$ with the IPR $D_{5h}(6)\text{-}C_{80}$ and $I_h(7)\text{-}C_{80}$ cages, respectively. The former can be obtained by a single C_2 insertion to a hexagon of the latter.
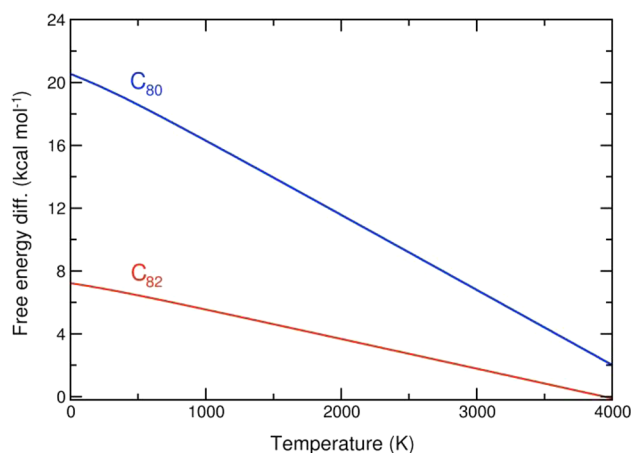
intimately related with one of the two observed isomers of $M_3N@C_{80}$, $I_h(7)\text{-}C_{80}$ and $D_{5h}(6)\text{-}C_{80}$. In fact, $Gd_3N@C_{2v}(39705)\text{-}C_{82}$ can be obtained from a single C_2 insertion to one hexagon of the prototypical $Gd_3N@I_h\text{-}C_{80}$, as pointed out by other authors;[8] analogously, $Gd_3N@C_s(39663)\text{-}C_{82}$ can be obtained from $Gd_3N@D_{5h}\text{-}C_{80}$. Therefore, it is possible that these C_{82}-based EMFs form from the C_{80} cages by C_2 insertion through the recently proposed closed network growth (CNG) mechanism.[31,32]

The close similarities between the topologies of the lowest-energy $Gd_3N@C_{80}$ and $Gd_3N@C_{82}$ EMFs help to understand
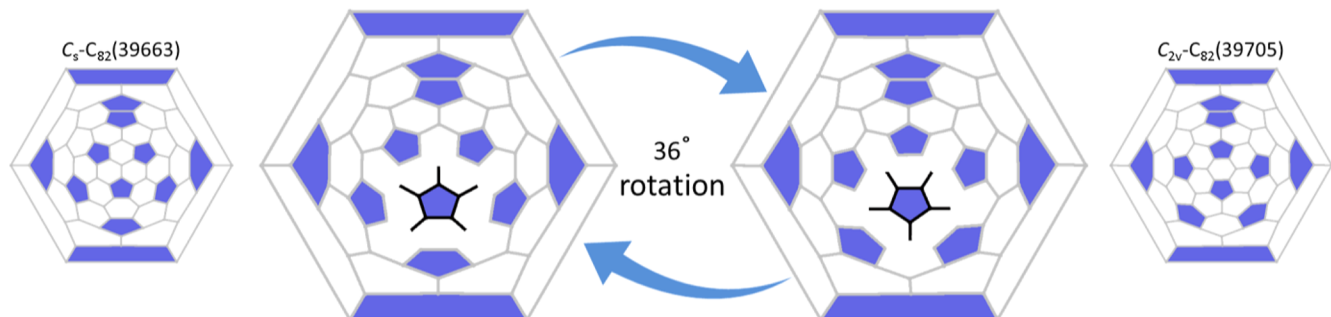
Figure 3. Schematic two-dimensional (Schlegel) representations of the $C_s(39663)\text{-}C_{82}$ and $C_{2v}(39705)\text{-}C_{82}$ cages showing the close similarities between them. The 36-degree rotation of the highlighted C_{10} pentagonal motif can be also seen as the 36-degree rotation of the C_{40} fragment (C_{10} + 30 C around it) that contains the central pentagon and five other pentagons surrounding it. It is the same relationship that exists between $I_h(7)\text{-}C_{80}$ and $D_{5h}(6)\text{-}C_{80}$.

1956

dx.doi.org/10.1021/ic302239e | *Inorg. Chem.* 2013, 52, 1954−1959

the effect of temperature on the predicted relative abundances of the isomers. We have computed the molar fractions and the free energy differences between the two hexaanionic $I_h(7)$-C_{80}^{6-} and $D_{5h}(6)$-C_{80}^{6-} cages for the range of temperatures between 0 and 4000 K. The predicted molar fractions are analogous (see Supporting Information) to those found by Slanina for the two isomers of $Sc_3N@C_{80}$,[14] that is, the relative abundance of $D_{5h}(6)$-C_{80}^{6-} with respect to $I_h(7)$-C_{80}^{6-} increases with temperature resulting in a 0.15/0.85 ratio at 2500 K. These two isomers, which are also related by a 36-degree rotation of a pentagonal motif, show the same C_{40} caps, and they only differ in the region connecting the two caps (see Supporting Information), with $I_h(7)$-C_{80} showing no pyracylene motifs and $D_{5h}(6)$-C_{80} showing five of them. From these results, therefore, one could infer that those cages with *higher number of pyracylenes* are favored at higher temperatures. The free energy difference between these two isomers as a function of temperature is plotted in Figure 5 (blue line). The difference

Table 3. Slopes of the Rotational (Rot) and Vibrational (Vib) Contributions to the Free Energy Differences with Respect to $I_h(7)$-C_{80}^{6-} for the IPR C_{80}^{6-} Isomers (1−6) as a Function of Temperature, along with the Symmetry Index (σ), the Number of Pyracylene Units (Pyra), and the Point Group for Each Isomer (Sym)[a,b]

Iso	Sym	σ	Pyra	Rot[a]	Vib[a]
1	D_{5d}	10	20	3.57	13.20
2	D_2	4	18	5.38	5.31
3	C_{2v}	2	13	6.75	4.44
4	D_3	6	15	4.57	4.42
5	C_{2v}	2	9	6.75	2.91
6	D_{5h}	10	5	3.55	1.08
7	I_h	60	0	0.00	0.00

[a]Units for the slopes are in $cal \cdot mol^{-1} \cdot K^{-1}$. [b]The absolute values of the slopes of the plots in Supporting Information, Figures S5 and S6 are shown.

Figure 5. Free energy difference (in $kcal \cdot mol^{-1}$) as a function of temperature for $C_s(39663)$-C_{82}^{6-} and $C_{2v}(39705)$-C_{82}^{6-} (red line) and $D_{5h}(6)$-C_{80}^{6-} and $I_h(7)$-C_{80}^{6-} (blue line).

at 0 K of around 20 $kcal \cdot mol^{-1}$ is reduced to only 2 at 4000 K (approximate slope of -4.50 $cal \cdot mol^{-1} \cdot K^{-1}$). The two related C_{82} cages, $C_{2v}(39705)$-C_{82} and $C_s(39663)$-C_{82}, show instead two and four pyracylene motifs, respectively. The difference at 0 K, around 7 $kcal \cdot mol^{-1}$, becomes negative, that is, inversion of relative abundance, at a temperature near 4000 K (approximate slope of -1.75 $cal \cdot mol^{-1} \cdot K^{-1}$). Remarkably, the slope *per pyracylene unit* is around 0.9 $cal \cdot mol^{-1} \cdot K^{-1}$ for the two free energy differences plotted in Figure 5. However, a more detailed analysis of the contributions to the free energy differences for these C_{80} and C_{82} isomers shows that both the rotational and the vibrational parts contribute significantly. On one hand, those isomers with lower symmetries are favored at higher temperatures, as can be easily understood from an inspection of the rotational partition function. The rotational contribution to the free energy difference is mainly a consequence of the different symmetry of the isomers (see Table 3 and Supporting Information). On the other hand, we also observe that there is a correlation between the vibrational contribution to the free energy difference and the number of pyracylene units. Those isomers with larger number of pyracylenes are more favored at higher temperatures (see Table 3 and Supporting Information). An inspection of the normal modes of vibration for the different isomers, which are

largely delocalized on the whole cage, does not allow a simple explanation in terms of characteristic topological patterns though.

Besides the relationships already mentioned between the IPR $D_{5h}(6)$-C_{80} and $I_h(7)$-C_{80} and the non-IPR $C_s(39663)$-C_{82} and $C_{2v}(39705)$-C_{82} structures, these four cages are also related to other C_{80}, C_{82}, and C_{84} isomers that encapsulate a wide variety of metal atoms or metal clusters as schematically depicted in Figure 6. Cages $C_s(39663)$-C_{82} and $C_{2v}(39705)$-C_{82} convert to $C_s(6)$-C_{82} and $C_{3v}(8)$-C_{82}, respectively, after a single Stone–Wales (SW) transformation in one pyracylene motif near the pentalene, see Scheme 1 and Figure 6. Moreover, the latter two cages can be interconverted by means of two SW isomerizations. The non-IPR $C_s(51365)$-C_{84} can be obtained from $C_s(39663)$-C_{82} after a C_2 insertion and two SW transformations. The structures shown in Figure 6 represent an important fraction of all the EMFs characterized so far. These apparently different structures share a common fragment with the $I_h(7)$-C_{80} cage, which ensures maximum separation between pentagons,[12] and only rather small modifications of this prototypical structure lead to other stable EMFs.

■ CONCLUSIONS

The incorporation of thermal contributions in the computations is necessary to explain the formation of $Gd_3N@C_s(39663)$-C_{82} at high temperatures, a non-IPR nitride EMF that was characterized by X-ray crystallography. Therefore, the formation of this EMF is also thermodynamically controlled as for other nitride, carbide, oxide, and sulfide EMFs. These results also show that $Gd_3N@C_{2v}(39705)$-C_{82} could be also detected in future experiments. Furthermore, close similarities exist between the cages of the lowest-energy $Gd_3N@C_{80}$ and $Gd_3N@C_{82}$ EMFs, which are related by insertion/extrusion of a single C_2 fragment. In fact, several C_{80}, C_{82}, and C_{84} isomers that encapsulate a wide variety of metal clusters and share common motifs with the prototypical $I_h(7)$-C_{80} are related by C_2 insertions/extrusions and SW transformations. We also find that both rotational (different symmetries) and vibrational contributions (different topologies) are significant to explain the free energy differences between the isomers within the same C_{2n} family of EMFs.
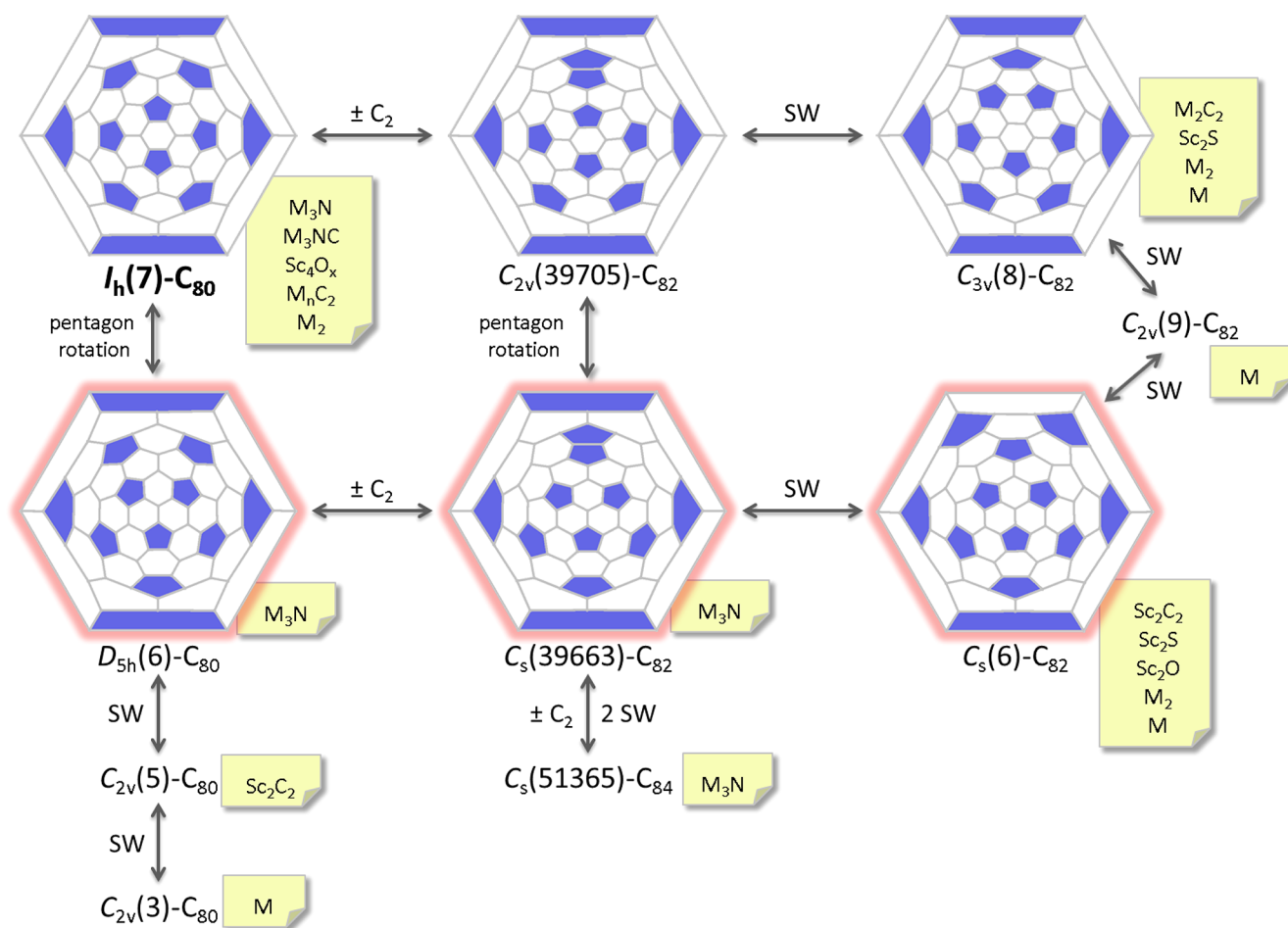
Figure 6. Schematic representation showing the connections between the different IPR and non-IPR structures of the C_{80}, C_{82}, and C_{84} families that are seen to encapsulate metal atoms or metal clusters. SW stands for Stone−Wales isomerization. The clusters that are seen encapsulated within each of these structures are also shown. The EMFs derived from these structures represent an important fraction of all the EMFs reported so far. The prototypical $I_h(7)$-C_{80} cage, which shares an important part of the structure with the other cages thus ensuring maximum separation of pentagons, is shown at the left top part of the figure. The cages in the central part of the figure, with the contour highlighted in red, $D_{5h}(6)$-C_{80}, $C_s(39663)$-C_{82}, and $C_s(6)$-C_{82}, are those favored at high temperatures compared to the cages at the top part.

Scheme 1. Stone−Wales Isomerization: Interconversion between Two Pyracylene Motifs
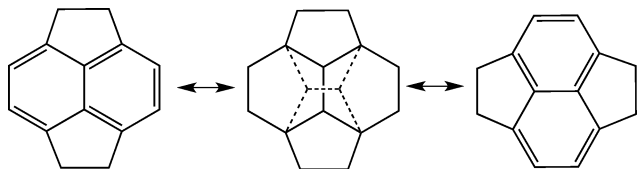
ASSOCIATED CONTENT

Ⓢ Supporting Information

Cartesian coordinates for the optimized structures, plots of molar fractions and free energy differences as functions of temperature (rotational and vibrational contributions) for isomers of the C_{80} and C_{82} families, and scheme showing the structural differences between the $I_h(7)$-C_{80} and $D_{5h}(6)$-C_{80} isomers. This material is available free of charge via the Internet at http://pubs.acs.org.

AUTHOR INFORMATION

Corresponding Author

*E-mail: antonio.rodriguezf@urv.cat (A.R.-F.), josepmaria.poblet@urv.cat (J.M.P.).

Notes

The authors declare no competing financial interest.

DEDICATION

†Dedicated to the Memory of Christian G. Claessens.

REFERENCES

(1) Chaur, M. N.; Melin, F.; Ortiz, A. L.; Echegoyen, L. *Angew. Chem., Int. Ed.* **2009**, *48*, 7514−7538.
(2) Dunsch, L.; Yang, S. *Small* **2007**, *3*, 1298−1320.
(3) Martin, N. *Chem. Commun.* **2006**, 2093−2104.
(4) Stevenson, S.; Rice, G.; Glass, T.; Harich, K.; Cromer, F.; Jordan, M. R.; Craft, J.; Hadju, E.; Bible, R.; Olmstead, M. M.; Maitra, K.; Fisher, A. J.; Balch, A. L.; Dorn, H. C. *Nature* **1999**, *401*, 55−57.
(5) Popov, A. A. *J. Comput. Theor. Nanosci.* **2009**, *6*, 292−317.

(6) Rodriguez-Fortea, A.; Balch, A. L.; Poblet, J. M. *Chem. Soc. Rev.* **2011**, *40*, 3551−3563.

(7) Yamada, M.; Akasaka, T.; Nagase, S. *Acc. Chem. Res.* **2009**, *43*, 92−102.

(8) Popov, A. A.; Dunsch, L. *J. Am. Chem. Soc.* **2007**, *129*, 11835−11849.

(9) Fowler, P. W.; Manolopoulos, D. E. *An Atlas of Fullerenes*; Oxford University Press: Oxford, U.K., 1995.

(10) Campanera, J. M.; Bo, C.; Poblet, J. M. *Angew. Chem., Int. Ed.* **2005**, *44*, 7230−7233.

(11) Valencia, R.; Rodriguez-Fortea, A.; Poblet, J. M. *Chem. Commun.* **2007**, 4161−4163.

(12) Rodriguez-Fortea, A.; Alegret, N.; Balch, A. L.; Poblet, J. M. *Nat. Chem.* **2010**, *2*, 955−961.

(13) Slanina, Z.; Lee, S. L.; Uhlik, F.; Adamowicz, L.; Nagase, S. *Theor. Chem. Acc.* **2007**, *117*, 315−322.

(14) Slanina, Z.; Nagase, S. *ChemPhysChem* **2005**, *6*, 2060−2063.

(15) Mercado, B. Q.; Stuart, M. A.; Mackey, M. A.; Pickens, J. E.; Confait, B. S.; Stevenson, S.; Easterling, M. L.; Valencia, R.; Rodriguez-Fortea, A.; Poblet, J. M.; Olmstead, M. M.; Balch, A. L. *J. Am. Chem. Soc.* **2010**, *132*, 12098−12105.

(16) Mercado, B. Q.; Chen, N.; Rodriguez-Fortea, A.; Mackey, M. A.; Stevenson, S.; Echegoyen, L.; Poblet, J. M.; Olmstead, M. M.; Balch, A. L. *J. Am. Chem. Soc.* **2011**, *133*, 6752−6760.

(17) Sun, M. L.; Slanina, Z.; Lee, S. L.; Uhlik, F.; Adamowicz, L. *Chem. Phys. Lett.* **1995**, *246*, 66−72.

(18) Hennrich, F. H.; Michel, R. H.; Fischer, A.; Richard-Schneider, S.; Gilb, S.; Kappes, M. M.; Fuchs, D.; Bürk, M.; Kobayashi, K.; Nagase, S. *Angew. Chem., Int. Ed. Engl.* **1996**, *35*, 1732−1734.

(19) Wang, C.-R.; Sugai, T.; Kai, T.; Tomiyama, T.; Shinohara, H. *Chem. Commun.* **2000**, 557−558.

(20) Mercado, B. Q.; Beavers, C. M.; Olmstead, M. M.; Chaur, M. N.; Walker, K.; Holloway, B. C.; Echegoyen, L.; Balch, A. L. *J. Am. Chem. Soc.* **2008**, *130*, 7854−7855.

(21) *ADF 2009.01*; Department of Theoretical Chemistry, Vrije Universiteit: Amsterda, The Netherlands, 2009.

(22) te Velde, G. T.; Bickelhaupt, F. M.; Baerends, E. J.; Guerra, C. F.; Van Gisbergen, S. J. A.; Snijders, J. G.; Ziegler, T. *J. Comput. Chem.* **2001**, *22*, 931−967.

(23) Becke, A. D. *Phys. Rev. A* **1988**, *38*, 3098−3100.

(24) Perdew, J. P. *Phys. Rev. B* **1986**, *33*, 8822−8824.

(25) Zhang, Y.; Yang, W. *Phys. Rev. Lett.* **1998**, *80*, 890−890.

(26) Becke, A. D. *J. Chem. Phys.* **1993**, *98*, 5648−5652.

(27) Grimme, S.; Antony, J.; Ehrlich, S.; Krieg, H. *J. Chem. Phys.* **2010**, *132*, 154104−154119.

(28) Andrae, D.; Haussermann, U.; Dolg, M.; Stoll, H.; Preuss, H. *Theor. Chim. Acta* **1990**, *77*, 123−141.

(29) Ahlrichs, R.; Bär, M.; Häser, M.; Horn, H.; Kölmel, C. *Chem. Phys. Lett.* **1989**, *162*, 165−169.

(30) Valencia, R.; Rodriguez-Fortea, A.; Clotet, A.; de Graaf, C.; Chaur, M. N.; Echegoyen, L.; Poblet, J. M. *Chem.—Eur. J.* **2009**, *15*, 10997−11009.

(31) Dunk, P. W.; Kaiser, N. K.; Hendrickson, C. L.; Quinn, J. P.; Ewels, C. P.; Nakanishi, Y.; Sasaki, Y.; Shinohara, H.; Marshall, A. G.; Kroto, H. W. *Nat. Commun.* **2012**, *3*, 855.

(32) Dunk, P. W.; Kaiser, N. K.; Mulet-Gas, M.; Rodriguez-Fortea, A.; Poblet, J. M.; Shinohara, H.; Hendrickson, C. L.; Marshall, A. G.; Kroto, H. W. *J. Am. Chem. Soc.* **2012**, *134*, 9380−9389.